AIP Journal of Applied Physics

Silicon nanocrystals with high boron and phosphorus concentration hydrophilic shell—Raman scattering and X-ray photoelectron spectroscopic studies

Minoru Fujii, Hiroshi Sugimoto, Masataka Hasegawa, and Kenji Imakita

Citation: Journal of Applied Physics **115**, 084301 (2014); doi: 10.1063/1.4866497
View online: http://dx.doi.org/10.1063/1.4866497
View Table of Contents: http://scitation.aip.org/content/aip/journal/jap/115/8?ver=pdfcov
Published by the AIP Publishing

Silicon nanocrystals with high boron and phosphorus concentration hydrophilic shell—Raman scattering and X-ray photoelectron spectroscopic studies

Minoru Fujii,[a] Hiroshi Sugimoto, Masataka Hasegawa, and Kenji Imakita
Department of Electrical and Electronic Engineering, Graduate School of Engineering, Kobe University, Rokkodai, Nada, Kobe 657-8501, Japan

(Received 26 December 2013; accepted 10 February 2014; published online 24 February 2014)

Boron (B) and phosphorus (P) codoped silicon (Si) nanocrystals, which exhibit very wide range tunable luminescence due to the donor to acceptor transitions and can be dispersed in polar liquids without organic ligands, are studied by Raman scattering and X-ray photoelectron spectroscopies. Codoped Si nanocrystals exhibit a Raman spectrum significantly different from those of intrinsic ones. First, the Raman peak energy is almost insensitive to the size and is very close to that of bulk Si crystal in the diameter range of 2.7 to 14 nm. Second, the peak is much broader than that of intrinsic ones. Furthermore, an additional broad peak, the intensity of which is about 20% of the main peak, appears around 650 cm^{-1}. The peak can be assigned to local vibrational modes of substitutional B and B-P pairs, B clusters, B-interstitial clusters, etc. in Si crystal. The Raman and X-ray photoelectron spectroscopic studies suggest that a crystalline shell heavily doped with these species is formed at the surface of a codoped Si nanocrystal and it induces the specific properties, i.e., hydrophilicity, high-stability in water, high resistance to hydrofluoric acid, etc. © *2014 AIP Publishing LLC*. [http://dx.doi.org/10.1063/1.4866497]

I. INTRODUCTION

Colloidal Si nanocrystals have been attracting significant attention because they can be a key material for Si-based printable electronics and are expected to be more suitable for biological applications than compound semiconductor nanocrystals due to the non-toxicity as a chemical element. The quality, i.e., size distribution, luminescence quantum efficiency, etc., of Si nanocrystals has been improved rapidly[1–5] and several kinds of electronic devices have been demonstrated.[6–11] In colloidal semiconductor nanocrystals, the surface termination is an important parameter to control the electronic states as well as the chemistry. In general, the surface of Si nanocrystals is functionalized by organic ligands to prevent agglomeration of nanocrystals in solution by the steric barriers. However, the surface molecules act as tunneling barriers for carrier transport in films produced from colloidal solutions and the films are usually capacitive. One of the approaches to realize high conductivity nanocrystal films from colloids is to replace organic ligands with inorganic ones. Although the ligand exchange process has been successfully applied in compound semiconductor nanocrystals,[12–14] it is not applicable to Si nanocrystals because Si forms covalent bonds with capping ligands. In Si nanocrystals, physical processes such as pulsed laser irradiation and microplasma treatments in solutions are applied to achieve the inorganic termination and to make them dispersible in polar solvents.[15]

Recently, we have developed a new method to produce Si nanocrystals dispersible in polar solvents without organic ligands.[16–18] The method is the formation of very high B and P concentration layers at the surface of Si nanocrystals. The layer induces negative potential at the surface and prevents the agglomeration by electrostatic repulsions. The colloidal solution of codoped Si nanocrystals is stable for years in methanol and exhibits efficient size-controllable photoluminescence (PL) in a very wide energy range (0.85–1.9 eV) due to the donor to acceptor transitions.[19] The efficient and relatively long lifetime luminescence of codoped Si nanocrystals suggests that majority of them are perfectly compensated and they have no charge carriers. Therefore, codoped Si nanocrystals can be regarded as a kind of intrinsic Si nanocrystals with additional functionalities such as extended tunable range of the luminescence energy and high solution dispersibility. For example, codoped Si nanocrystals are dispersed in water without organic capping and exhibit efficient PL in a biological window.[20] This is an attractive feature as a contrast agent in bioimaging.

Although the strategy that solution dispersion of semiconductor nanocrystals is achieved by the formation of a high impurity concentration shell is unique and worth studying in detail, little is known about the structure of the high B and P concentration shell. The purpose of this work is to clarify the structure, especially that of the shell, of B and P codoped Si nanocrystals. Raman spectroscopy is known to be a powerful tool to study the bonding states and symmetry of impurities in Si crystal[21] and different kinds of local vibrational modes have been identified.[21–23] Raman spectroscopy is also widely used for the characterization of Si nanocrystals, because the spectral shape is sensitive to the size.[24–26] In this work, we study the structure of B and P codoped Si nanocrystals by Raman spectroscopy and X-ray photoelectron spectroscopy (XPS). We show that the Raman

[a]Author to whom correspondence should be addressed. Electronic mail: fujii@eedept.kobe-u.ac.jp. Tel.: +81-78-803-6081.

spectra of codoped Si nanocrystals are significantly different from those of intrinsic ones. In particular, codoped Si nanocrystals exhibit relatively strong Raman signals assigned to local vibrational modes of substitutional B, P and B-P pairs, B clusters, B-interstitial clusters, etc., in Si crystal. The present results provide clear evidences for the existence of a crystalline shell doped with different kinds of B and P related species at the surface of a codoped Si nanocrystal.

II. EXPERIMENTAL

Impurity-doped Si nanocrystals were prepared by a co-sputtering method. Detailed preparation procedure is described in our previous papers.[16,17] Si and SiO_2 are simultaneously sputter-deposited and annealed to grow Si nanocrystals in silica matrices. For the growth of B or P doped Si nanocrystals, phosphosilicate glass (PSG) or borosilicate glass (BSG), respectively, are added to the sputtering targets. This results in the formation of P (B) doped Si nanocrystals in PSG (BSG) matrices.[27,28] For the growth of codoped Si nanocrystals, Si, SiO_2, PSG, and BSG were simultaneously sputter-deposited and annealed. In this case, codoped Si nanocrystals are grown in borophosphosilicate glass (BPSG) matrices.[29] To isolate Si nanocrystals from silica or silicate matrices, samples are dissolved in hydrofluoric acid (HF) solutions (46 wt. %) for 1 h. Isolated nanocrystals were then transferred to methanol. It should be stressed here that undoped, P-doped and B-doped Si nanocrystals agglomerate in methanol and form large precipitates. On the other hand, in codoped samples, precipitates are hardly observed and majority of nanocrystals are dispersed in methanol. B and P concentration in codoped Si nanocrystals estimated by inductively coupled plasma atomic emission spectrometry (ICP-AES) measurements is 13–22 at. % and 0.8–4.4 at. %, respectively.[19] No clear dependence of the concentration on annealing temperature or size is observed.[19]

Raman spectra were measured using a confocal microscope (50× objective lens, NA = 0.8) equipped with a single monochromator and a charge coupled device (CCD). The excitation source was a 514.5 nm line of an Ar ion laser. The excitation power was 1 mW. The X-ray source for XPS measurements (PHI X-tool, ULVAC-PHI) was Al Kα. The samples for Raman scattering and XPS measurements were prepared by drop-coating nanocrystal-dispersed methanol on gold (Au)-coated Si wafers. TEM observations (JEM-2010, JEOL) were performed by dropping the solution on carbon-coated TEM meshes.

III. RESULTS AND DISCUSSION

Figure 1(a) shows a photograph of codoped colloidal Si nanocrystals. The solution is very clear due to agglomeration-free perfect dispersion of nanocrystals. Figure 1(b) shows a TEM image of codoped Si nanocrystals. Because of the perfect dispersion in solution, no three-dimensional agglomerates are observed. The lattice fringes in the high-resolution TEM (HRTEM) image (inset) correspond to (111) planes of Si crystal. The crystallinity is very high and almost all nanocrystals are single crystal. The diameter of codoped Si nanoparticles can be controlled from 1 to

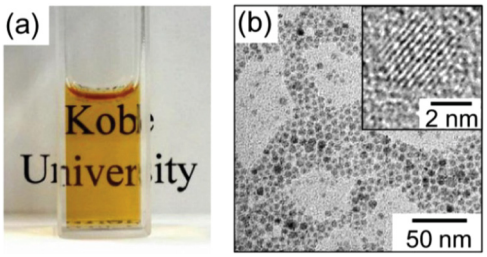

FIG. 1. (a) Photograph of B and P codoped colloidal Si nanocrystals (methanol solution). (b) TEM image and high-resolution TEM image (inset). The annealing temperature is 1200 °C.

14 nm by changing the annealing temperature (T_a) from 900 to 1300 °C. When the annealing temperature is below 1000 °C, amorphous particles are formed, while above 1050 °C, crystalline ones are grown.[19] In this work, we limit the annealing temperature range from 1050 to 1300 °C to focus on crystalline particles.

Figure 2(a) shows Raman spectra of B and P codoped Si nanocrystals annealed at different temperatures in BPSG matrices. As references, the spectra of intrinsic and B or P singly-doped Si nanocrystals in silica or silicate matrices grown at 1200 °C are shown. The intrinsic Si nanocrystals exhibit a Raman peak around 520 cm^{-1} with a tail at the low-wavenumber side. This is a typical Raman spectral shape of Si nanocrystals. The size dependence of the spectral shape has been studied in detail for many years.[24–26] The

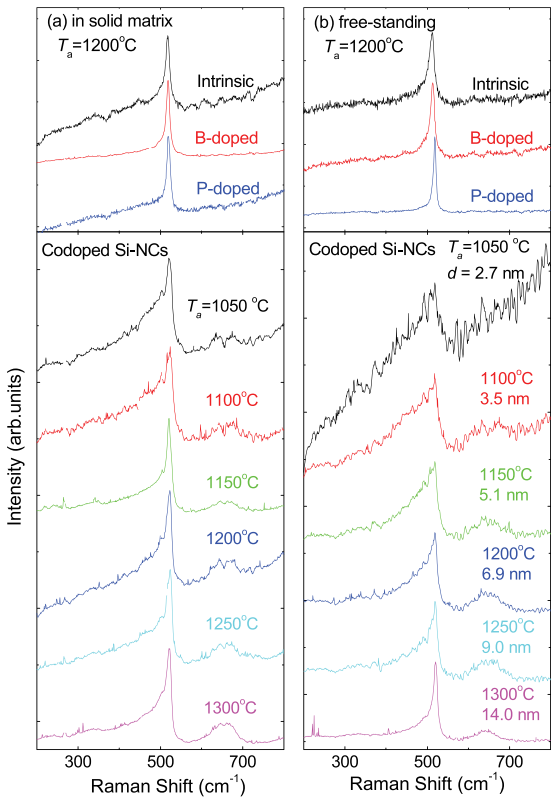

FIG. 2. (a) Raman spectra of B and P codoped Si nanocrystals in BPSG matrices. T_a is changed from 1050 to 1300 °C. Spectra of intrinsic, B-doped and P-doped Si nanocrystals in silica or silicate matrices are also shown. (b) Raman spectra after removing silica or silicate matrices by HF etching.

spectral shape of B or P singly doped Si nanocrystals is similar to that of intrinsic Si nanocrystals except for small differences in the peak wavenumbers and the widths. On the other hand, the Raman spectra of codoped Si nanocrystals are significantly different from that of the intrinsic one. First, despite high crystallinity evidenced by HRTEM images, the Raman peak is much broader. Furthermore, a broad peak appears around 650 cm^{-1}, which is not observed in intrinsic and B or P singly doped Si nanocrystals.

The Raman spectra of Si nanocrystals after removing silica or silicate matrices are shown in Fig. 2(b). The spectral shape of intrinsic and B or P singly doped Si nanocrystals does not change significantly by the removal of silica or silicate matrices. On the other hand, that of codoped Si nanocrystals changes in some aspects, especially when the annealing temperature is relatively low. The shape of the 520 cm^{-1} peak after etching is like a right-angled triangle with a gentle slope on the low-wavenumber side and a steep edge at the high-wavenumber side. The change of the spectral shape is probably due to the removal of relatively large Si nanocrystals in the size distribution during the process of extracting nanocrystals from matrices.[16] In contrast to the 520 cm^{-1} peak, the shape of the 650 cm^{-1} peak does not change significantly. In many cases, the intensity of the 650 cm^{-1} peak with respect to that of the 520 cm^{-1} one slightly increases after etching. The height of the 650 cm^{-1} peak is about 20% of that of the 520 cm^{-1} peak, when the annealing temperature is higher than 1100 °C. When the annealing temperature is 1050 °C, it is weaker but still observable.

Since the largest phonon energy of Si crystal is 520 cm^{-1}, the 650 cm^{-1} peak should be related to doped B and/or P. In Fig. 3, a Raman spectrum of free-standing codoped Si nanocrystals ($T_a = 1200$ °C) is compared with the wavenumbers of several kinds of B or P related local vibrational modes in Si crystal. One of the candidates of the 650 cm^{-1} peak is local vibrational modes of substitutional B.

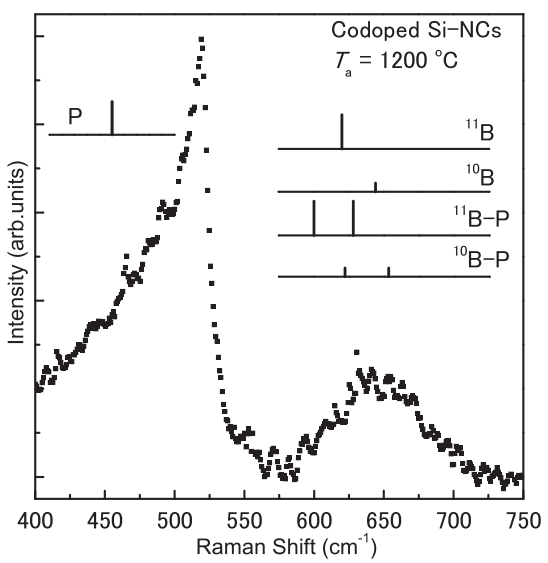

FIG. 3. Raman spectrum of free-standing B and P codoped Si nanocrystals. The wavenumbers of substitutional B, P, and B-P local vibrational modes in Si crystal are shown with vertical bars.

In heavily B doped bulk Si crystal, substitutional B atoms exhibit weak Raman peaks at 620 (^{11}B) and 644 cm^{-1} (^{10}B).[21,30] The intensity ratio of the peaks reflects natural abundance of ^{11}B (80.2%) and ^{10}B (19.8%) and is about 4:1. The B local modes are also observed in B doped Si nanowires[31] and nanocrystals,[32] although in the present B singly doped Si nanocrystals, the signal was below the detection limit. Another candidate of the 650 cm^{-1} peak is local vibrational modes of substitutional B-P pairs in Si crystal.[33,34] The comparison of the spectral shape and the wavenumbers of the local modes in Fig. 3 suggests that the B and B-P local vibrational modes partly contribute to the 650 cm^{-1} peak. However, they cannot explain the whole range of the broad 650 cm^{-1} peak.

Considering extremely high B concentration in codoped Si nanocrystals, it is very plausible that doped B atoms form clusters, e.g., B_2, and B-interstitial clusters, e.g., BI, B_2I, B_2I_2, etc, where B_nI_m refers to a cluster composed of n B atoms with m interstitials (B or Si). B clusters and B-interstitial clusters are known to be formed by B implantation in Si crystal.[22,23] Vibrational frequencies of these clusters in Si crystal have been studied experimentally and theoretically and some of them are within the broad 650 cm^{-1} peak.[22,23] Therefore, B clusters and B-interstitial clusters are strong candidates of the peak, although it is difficult to identify the kinds of clusters.

In codoped Si nanocrystals, a large amount of P is also doped.[19] This suggests that substitutional P and/or P-related clusters also contribute to the Raman spectra. Because of 11% larger mass of P than Si, they exhibit Raman peaks at the low wavenumber side of the main peak. In fact, the local vibrational mode of substitutional P in Si crystal is known to be around 441 cm^{-1} as designated in Fig. 3.[21] Although clear peaks are not observed, it is plausible that substitutional P and/or P-related clusters are the constituents of the extremely long low-wavenumber tail of the main peak.

In Fig. 4(a), the peak wavenumbers of codoped Si nanocrystals in BPSG matrices and free-standing ones are plotted as a function of the annealing temperature. The data of intrinsic Si nanocrystals are also shown as references. Intrinsic Si nanocrystals in silica matrices exhibit a Raman peak around 519 cm^{-1}, which is slightly lower than that of bulk Si crystal (520 cm^{-1}). By etching out silica matrices, the peak shifts to lower wavenumber and reaches 516 cm^{-1}. The low energy Raman peak of free-standing Si nanocrystals is generally explained by the phonon confinement effect.[24–26] The effect is partly compensated by compressive stress exerted from surrounding solid matrices.[24] This results in different Raman wavenumber between free-standing NCs and NCs in solid matrices.

The Raman peak wavenumbers of codoped Si nanocrystals are different from those of intrinsic ones. In BPSG matrices, the peak is in the range of 522 to 524 cm^{-1}. It shifts to lower wavenumber by removing BPSG matrices. This behavior is qualitatively similar to that of intrinsic Si nanocrystals. However, the peak wavenumber of free-standing codoped Si nanocrystals is much larger than that of intrinsic Si nanocrystals and is very close to that of bulk Si crystal. In Fig. 4(b), the peak wavenumber of codoped free-standing Si

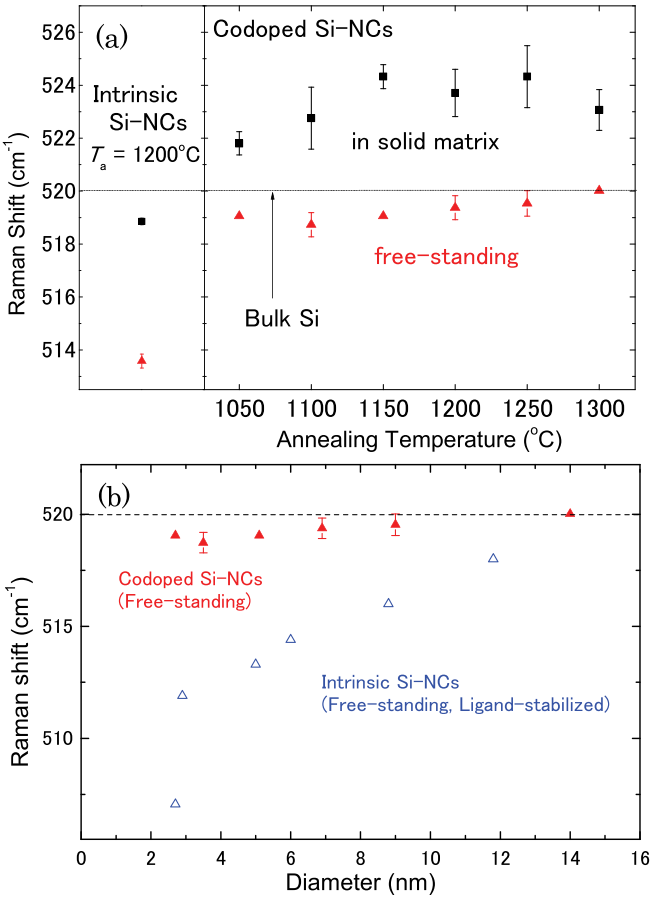

FIG. 4. (a) Raman peak wavenumbers of codoped Si nanocrystals in BPSG matrices and free-standing codoped Si nanocrystals as a function of annealing temperature. The data of intrinsic Si nanocrystals are also shown. (b) Raman peak wavenumber of free-standing codoped Si nanocrystals as a function of the diameter. The data of intrinsic ligand-stabilized Si nanocrystals taken from Ref. 24 are also shown.

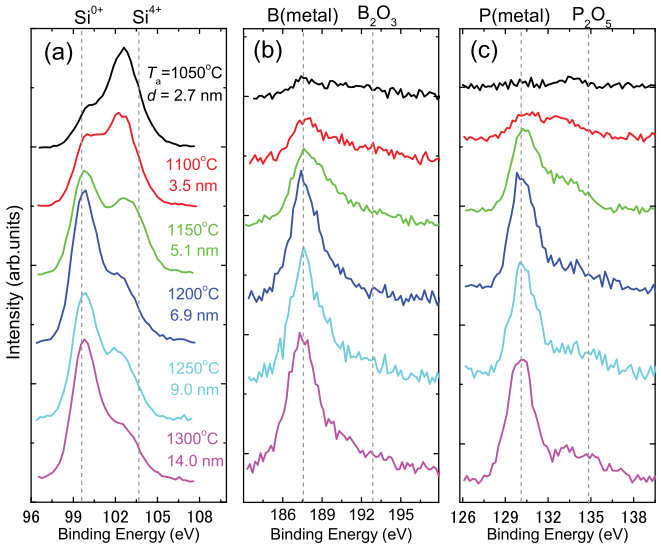

FIG. 5. (a) Si 2p, (b) B 1s, and (c) P 2p XPS spectra of B and P codoped Si nanocrystals prepared with different annealing temperatures. The annealing temperatures and the average diameters are shown in (a).

nanocrystals is plotted as a function of the diameter. For comparison, the data of ligand-stabilized free-standing intrinsic Si nanocrystals are shown.[24] In the ligand-stabilized Si nanocrystals, size-dependent low energy shift of the peak is clearly observed. The size dependence is well-explained by the phonon confinement effect. On the other hand, in codoped free-standing Si nanocrystals, the peak shifts only slightly from 520 cm^{-1} to 519 cm^{-1}, when the average diameter is decreased from 14 to 2.7 nm. The very small size dependence of the peak energy strongly suggests that, even after removing BPSG matrices, codoped Si nanocrystals have a hard shell and the low wavenumber shift of the Raman peak by the phonon confinement effect is compensated by compressive stress exerted from the shell.

In order to study the atomic structure of the shell of codoped Si nanocrystals, we measure the XPS spectra. Figure 5 shows XPS spectra of codoped free-standing Si nanocrystals prepared at different annealing temperatures. In the Si 2 p core signal (Fig. 5(a)), a peak assigned to Si nanocrystal cores (Si^0) and that to surface native oxides are observed around 99.8 and 102.6 eV, respectively. The binding energy of the oxides is smaller than that of stoichiometric SiO_2 (103.8 eV, Si^{4+} in Figure 5(a)) and is close to the value of Si^{3+} (102.7 eV).[35] This suggests that only Si atoms at the outermost surface have bonds with oxygen (O) atoms and the thickness of the oxide layer is less than a monolayer. The intensity of the oxide signal increases with decreasing the size. This can be explained qualitatively by the increase of the ratio of surface Si atoms within the escape depth of photoelectrons (~2 nm).[36]

Figure 5(b) shows the B 1 s signals. Boron metal and boron oxide (B_2O_3) exhibit XPS peaks at 187–188 and 193 eV, respectively.[37] The main peak in Fig. 5(b) is around 188 eV, indicating that majority of B atoms exist in Si nanocrystals in non-oxidized states. A tail towards higher energy suggests slight oxidation. Although the intensity of the 188 eV peak decreases and the spectrum becomes broad with decreasing the size, majority of B atoms are not oxidized even for the smallest nanocrystals. Similar results are obtained for the P 2p signals. In Figure 5(c), the main peak around 130 eV can be assigned to non-oxidized P atoms and the broad tail to suboxides. In contrast to the B 1s signal, the oxide-related signal is stronger than that of the non-oxidized one in the lowest temperature annealed samples. From the data in Fig. 5, we estimated the ratio of B to P in the shell. When the annealing temperature is higher than 1150 °C, the ratio is in the range of 3 to 4 and has no clear dependence on the annealing temperature. Below 1100 °C, the signal is too weak and noisy for quantitative discussion.

The data in Fig. 5 are obtained for samples one day after preparation. When the samples are kept in methanol for a long period, e.g., a year, oxidation slowly proceeds. The XPS peak of surface oxidized Si at 102.6 eV shifts to 104 eV (Si^{4+}) and the intensity with respect to that of the Si^0 peak increases. The thickness of oxides estimated from the intensity ratio of Si^{4+} and Si^0 peaks after one year storage in methanol is about 1 nm. Slight oxidation after long term storage is also observed for B and P. However, even after one year storage in methanol, signals from non-oxidized B and P are stronger than those of oxidized ones except for the P 2p peak of the sample annealed at 1050 °C.

The results of the XPS measurements, i.e., large amounts of non-oxidized B and P exist on and/or near the surface of codoped Si nanocrystals, are consistent with our model that crystalline Si shells heavily doped with B and/or P atoms are formed at the surface of nanocrystals.[19] However, the XPS data do not provide information on the bonding states of B and P in the shell because of small chemical shifts of borides and phosphides.

In B doped bulk Si crystal, it is well-known that saturated B-rich layers (BRL) are formed at the interface between B_2O_3 and Si after thermal treatments.[38,39] The BRL is hydrophilic and has high resistance to HF solution. These properties of BRL are similar to those of the shells in codoped Si nanocrystals. The shell is thus considered to be a kind of BRL. What is unknown at present is the role of P for the formation of the shell. In the present preparation procedure, doping of P in addition to B is indispensable for the shell formation.[18] One plausible explanation is that codoping of P stabilizes larger amount of B at the surface by charge compensation. Further research is necessary to fully understand the interplay of P and B for the formation of the shell.

IV. CONCLUSION

We demonstrate that B and P codoped Si nanocrystals exhibit Raman spectra significantly different from that of intrinsic Si nanocrystals. The Raman peak energy of free-standing codoped Si nanocrystals is almost independent of the size and is close to that of bulk Si crystal ($520\,cm^{-1}$) in the diameter range of 2.7 to 14 nm. Furthermore, the shape of the $520\,cm^{-1}$ peak is very much different from that of intrinsic Si nanocrystals. In addition, codoped Si nanocrystals have a broad Raman peak around $650\,cm^{-1}$, which is considered to arise from local vibrational modes of substitutional B and B-P pairs, B clusters, B-interstitial clusters, etc. XPS measurements demonstrate the existence of large amounts of non-oxidized B and P on and/or near the surface of codoped Si nanocrystals. The present results demonstrate that a thin hard crystalline shell containing large amounts of B and P related species are formed at the surface of a codoped Si nanocrystal and it induces the specific properties in solution.

ACKNOWLEDGMENTS

This work was supported by KAKENHI (Grant Nos. 23310077 and 24651143).

[1]A. Gupta, M. T. Swihart, and H. Wiggers, Adv. Funct. Mater. **19**, 696 (2009).
[2]L. Mangolini and U. Kortshagen, Adv. Mater. **19**, 2513 (2007).
[3]M. L. Mastronardi *et al.*, J. Am. Chem. Soc. **133**, 11928 (2011).
[4]M. L. Mastronardi, F. Maier-Flaig, D. Faulkner, E. J. Henderson, C. Kübel, U. Lemmer, and G. A. Ozin, Nano Lett. **12**, 337 (2012).
[5]C. M. Hessel, D. Reid, M. G. Panthani, M. R. Rasch, B. W. Goodfellow, J. Wei, H. Fujii, V. Akhavan, and B. A. Korgel, Chem. Mater. **24**, 393 (2012).
[6]M. L. Mastronardi *et al.*, Small **8**, 3647 (2012).
[7]K.-Y. Cheng, R. Anthony, U. R. Kortshagen, and R. J. Holmes, Nano Lett. **10**, 1154 (2010).
[8]K.-Y. Cheng, R. Anthony, U. R. Kortshagen, and R. J. Holmes, Nano Lett. **11**, 1952 (2011).
[9]D. P. Puzzo, E. J. Henderson, M. G. Helander, Z. Wang, G. A. Ozin, and Z. Lu, Nano Lett. **11**, 1585 (2011).
[10]V. Švrček, D. Mariotti, T. Nagai, Y. Shibata, I. Turkevych, and M. Kondo, J. Phys. Chem. C **115**, 5084 (2011).
[11]C.-C. Tu, L. Tang, J. Huang, A. Voutsas, and L. Y. Lin, Appl. Phys. Lett. **98**, 213102 (2011).
[12]A. Nag, M. V. Kovalenko, J.-S. Lee, W. Liu, B. Spokoyny, and D. V. Talapin, J. Am. Chem. Soc. **133**, 10612 (2011).
[13]J.-S. Lee, M. V. Kovalenko, J. Huang, D. S. Chung, and D. V. Talapin, Nat. Nanotechnol. **6**, 348 (2011).
[14]A. T. Fafarman *et al.*, J. Am. Chem. Soc. **133**, 15753 (2011).
[15]D. Mariotti, V. Švrček, J. W. J. Hamilton, M. Schmidt, and M. Kondo, Adv. Funct. Mater. **22**, 954 (2012).
[16]M. Fukuda, M. Fujii, H. Sugimoto, K. Imakita, and S. Hayashi, Opt. Lett. **36**, 4026 (2011).
[17]H. Sugimoto, M. Fujii, K. Imakita, S. Hayashi, and K. Akamatsu, J. Phys. Chem. C **116**, 17969 (2012).
[18]H. Sugimoto, M. Fujii, K. Imakita, S. Hayashi, and K. Akamatsu, J. Phys. Chem. C **117**, 6807 (2013).
[19]H. Sugimoto, M. Fujii, K. Imakita, S. Hayashi, and K. Akamatsu, J. Phys. Chem. C **117**, 11850 (2013).
[20]H. Sugimoto, M. Fujii, Y. Fukuda, K. Imakita, and K. Akamatsu, Nanoscale **6**, 122 (2014).
[21]A. Barker and A. Sievers, Rev. Mod. Phys. **47**, S1 (1975).
[22]J. Adey, J. P. Goss, R. Jones, and P. R. Briddon, Phys. Rev. B **67**, 245325 (2003).
[23]P. Deák, A. Gali, A. Sólyom, P. Ordejón, K. Kamarás, and G. Battistig, J. Phys.: Condens. Matter **15**, 4967 (2003).
[24]C. M. Hessel, J. Wei, D. Reid, H. Fujii, M. C. Downer, and B. A. Korgel, J. Phys. Chem. Lett. **3**, 1089 (2012).
[25]H. Richter, Z. P. Wang, and L. Ley, Solid State Commun. **39**, 625 (1981).
[26]I. H. Campbell and P. M. Fauchet, Solid State Commun. **58**, 739 (1986).
[27]M. Fujii, S. Hayashi, and K. Yamamoto, J. Appl. Phys. **83**, 7953 (1998).
[28]M. Fujii, A. Mimura, S. Hayashi, and K. Yamamoto, Appl. Phys. Lett. **75**, 184 (1999).
[29]M. Fujii, K. Toshikiyo, Y. Takase, Y. Yamaguchi, and S. Hayashi, J. Appl. Phys. **94**, 1990 (2003).
[30]F. Cerdeira, T. Fjeldly, and M. Cardona, Phys. Rev. B **9**, 4344 (1974).
[31]T. Kawashima, G. Imamura, T. Saitoh, K. Komori, M. Fujii, and S. Hayashi, J. Phys. Chem. C **111**, 15160 (2007).
[32]K. Sato, N. Fukata, and K. Hirakuri, Appl. Phys. Lett. **94**, 161902 (2009).
[33]R. C. Newman and R. S. Smith, Solid State Commun. **5**, 723 (1967).
[34]V. Tsvetov, Appl. Phys. Lett. **10**, 326 (1967).
[35]S. M. A. Durrani, M. F. Al-Kuhaili, and E. E. Khawaja, J. Phys.: Condens. Matter **15**, 8123 (2003).
[36]Z. H. Lu, J. P. McCaffrey, B. Brar, G. D. Wilk, R. M. Wallace, L. C. Feldman, and S. P. Tay, Appl. Phys. Lett. **71**, 2764 (1997).
[37]A. K.-V. Alexander, V. Naumkin, S. W. Gaarenstroom, and Cedric J. Powell, NIST Standard Reference Database 20, Version 4.1 (web version), 2012, see http:/srdata.nist.gov/xps/.
[38]M. A. Kessler, T. Ohrdes, B. Wolpensinger, and N.-P. Harder, Semicond. Sci. Technol. **25**, 055001 (2010).
[39]E. Arai, H. Nakamura, and Y. Terunuma, J. Electrochem. Soc. **120**, 980 (1973).